



THE UNIVERSITY *of* EDINBURGH

Edinburgh Research Explorer

## The power-law relation between inclusion aspect ratio and porosity: Implications for electrical and elastic modeling

### Citation for published version:

Chapman, M & Cilli, PA 2020, 'The power-law relation between inclusion aspect ratio and porosity: Implications for electrical and elastic modeling', *Journal of Geophysical Research. Solid Earth*.  
<https://doi.org/10.1029/2019JB019187>

### Digital Object Identifier (DOI):

[10.1029/2019JB019187](https://doi.org/10.1029/2019JB019187)

### Link:

[Link to publication record in Edinburgh Research Explorer](#)

### Document Version:

Peer reviewed version

### Published In:

Journal of Geophysical Research. Solid Earth

### General rights

Copyright for the publications made accessible via the Edinburgh Research Explorer is retained by the author(s) and / or other copyright owners and it is a condition of accessing these publications that users recognise and abide by the legal requirements associated with these rights.

### Take down policy

The University of Edinburgh has made every reasonable effort to ensure that Edinburgh Research Explorer content complies with UK legislation. If you believe that the public display of this file breaches copyright please contact [openaccess@ed.ac.uk](mailto:openaccess@ed.ac.uk) providing details, and we will remove access to the work immediately and investigate your claim.



1     **The power-law relation between inclusion aspect ratio**  
2     **and porosity: Implications for electrical and elastic**  
3     **modeling**

4                     **P. A. Cilli<sup>1,2\*</sup>, M. Chapman<sup>1,2</sup>**

5             <sup>1</sup>Grant Institute, School of GeoSciences, The University of Edinburgh, James Hutton Rd, King's  
6                     Buildings, Edinburgh, EH9 3FE, UK.

7                     <sup>2</sup>International Centre for Carbonate Reservoirs, Edinburgh, UK.

8             **Key Points:**

- 9             • The differential effective medium model aspect ratio appears to follow a power-  
10             law with porosity
- 11            • Introducing a power-law relation leads to improved modeling of 7 public domain  
12             data sets
- 13            • Introducing a power-law relation leads to alternative models for 5 empirical mod-  
14             els

---

\*Current address: Department of Earth Sciences, University of Oxford, South Parks Road, Oxford, OX1  
3AN, UK

Corresponding author: Phil Cilli, [phillip.cilli@earth.ox.ac.uk](mailto:phillip.cilli@earth.ox.ac.uk)

15 **Abstract**

16 Geophysicists depend on rock physics relationships to interpret resistivity and seismic  
 17 velocity in terms of rock porosity, but it has proven difficult to capture the effect of pore  
 18 geometry on such relations through simple and easy to apply formulae. Inclusion mod-  
 19 eling relates moduli to porosity through an equivalent grain or pore aspect ratio but of-  
 20 ten fails to account for observed trends, whereas empirical relations can be hard to ex-  
 21 trapolate beyond their range of validity, often giving incorrect results in the low and high  
 22 porosity limits. We show that introducing a power-law relationship between porosity and  
 23 equivalent grain or pore aspect ratio allows inclusion models to reproduce 5 published  
 24 empirical resistivity-porosity and velocity-porosity relationships, providing a first prin-  
 25 ciples basis for extrapolation to other cases of interest. We find the deviation of resis-  
 26 tivity from Archie’s law in carbonates is related to a systematic change of grain shape  
 27 with porosity, and we derive a new relation which fits carbonate resistivity data with sim-  
 28 ilar accuracy to the Humble equation while being correct at high porosity. We then ob-  
 29 tain an analog for the Castagna and Pickett relationships for wet, calcitic rocks, which  
 30 is valid in the low and high porosity limits, giving rise to a new, physically derived  $V_p/V_s$   
 31 versus porosity model.

32 **1 Introduction**

33 An ongoing challenge in rock physics modeling is understanding how electrical and  
 34 elastic properties vary with porosity for various rock types. For electrical resistivity, Archie’s  
 35 (Archie, 1942) law is widely believed to produce acceptable results in clean sandstones  
 36 (Glover, Hole, & Pous, 2000). The electrical properties of carbonates, however, are sig-  
 37 nificantly more complex; a property usually attributed to the diversity of pore types present  
 38 (Focke & Munn, 1987; Saleh & Castagna, 2004; Salem & Chilingarian, 1999). A mod-  
 39 ification of Archie’s first law, the Humble (Winsauer, Shearin Jr, Masson, & Williams,  
 40 1952) equation, may be more accurate in the case of complex pore geometries, but is in-  
 41 correct in the high-porosity limit. Other models, such as the Shell (Neustaedter, 1968)  
 42 model, the Borai et al. (1987) model, and the Focke and Munn (1987) relations, are pop-  
 43 ular in modeling the electrical properties of carbonates, however they are all empirical  
 44 modifications of Archie’s first law, and are not evidently grounded in first-principles physics.

45 Rock physics models derived from first principles may have the benefit of extrap-  
 46 olating to various rock types, unlike these empirical models which are only applicable

47 to the rocks where they were calibrated. First principles resistivity models for carbon-  
48 ate rocks, however, are much less developed. In the case of inclusion modeling (Eshelby,  
49 1957), this is due to the difficulty in approximating carbonate grains or pores with spheres  
50 and ellipsoids. A notable inclusion model designed specifically for carbonates is that of  
51 Xu and Payne (2009).

52 Just as the electrical properties of carbonates vary with pore types present, the elas-  
53 tic properties of carbonates are also severely dependent on the pore types present. Anal-  
54 ogously to the electrical modeling case, significant progress has been made in modeling  
55 velocity-porosity trends in the siliciclastic environment (E.g., Dvorkin and Nur (1996);  
56 D.-H. Han, Nur, and Morgan (1986); Raymer, Hunt, and Gardner (1980); Vernik and  
57 Nur (1992)), however modeling the properties of carbonates, has proven to be more com-  
58 plex (Kittridge, 2014).

59 Modulus-porosity trends are produced using a range of tools, including empirical,  
60 bounding, and inclusions methods. Empirical methods (E.g., Castagna, Batzle, and Kan  
61 (1993); D.-H. Han et al. (1986); Pickett (1963)) are useful but challenging to extrapo-  
62 late beyond their pre-calibrated rock types. Bounding average (E.g., Hill (1952)) and mod-  
63 ified bound (E.g., A. Nur, Mavko, Dvorkin, and Galmudi (1998); A. M. Nur, Mavko, Dvorkin,  
64 and Gal (1995)) methods can yield comparable accuracy to more sophisticated models  
65 (Man & Huang, 2011; Zimmerman, 1991), but can suppress important dependencies on  
66 microstructure. As in the electrical modeling case, elastic inclusion models (E.g., Berry-  
67 man (1980); Kuster and Toksöz (1974); Norris (1985)) are often not preferred since the  
68 advantages of having a physics-based approach can be outweighed by the unrealistic as-  
69 sumptions made about the pore geometry. Pride et al. (2017) provide analytical rock physics  
70 models which focus on the relationship between effective pressure the electrical and elas-  
71 tic properties of a cracked, porous rock by modeling how porosity changes with pressure,  
72 in combination with how moduli change with porosity.

73 Given that the electrical and elastic properties of rocks are influenced by pore or  
74 grain geometry, obtaining realistic carbonate rock physics trends may require character-  
75 izing these geometries, which is a prevailing challenge in carbonate rock physics (Ansel-  
76 metti & Eberli, 1993, 1999; Eberli, Baechle, Anselmetti, & Incze, 2003; Focke & Munn,  
77 1987; Fournier et al., 2018). Some have proposed incorporating pore geometry effects into  
78 modeling by using inclusion models with a porosity-dependent pore or grain aspect ra-

79 tio (Kazatchenko, Markov, & Mousatov, 2004; Kazatchenko, Markov, Mousatov, Per-  
 80 vago, et al., 2006; Markov, Kazatchenko, Mousatov, et al., 2004). An aspect ratio which  
 81 is piecewise-constant in porosity was proposed by Kazatchenko et al. (2004), while quadratic  
 82 trends in porosity were considered by Aquino-López, Mousatov, and Markov (2011) and  
 83 Aquino-López, Mousatov, Markov, and Kazatchenko (2015). More recently, Ellis and Kirstet-  
 84 ter (2018) proposed a logarithmic trend between aspect ratio and porosity.

85 This paper argues for the adoption of a power-law relationship between pore or grain  
 86 aspect ratio and porosity. We show the power-law relationship, combined with a differ-  
 87 ential effective medium (DEM) model, fits 7 electrical and elastic data sets with lower  
 88 misfit than the single aspect ratio DEM model. This power-law model approximates the  
 89 empirical resistivity-porosity model of Focke and Munn (1987) for carbonates, and has  
 90 comparable accuracy to the Humble (Winsauer et al., 1952) equation in the range of mea-  
 91 sured data while being correct at high porosities like Archie’s (Archie, 1942) first law.  
 92 Through this power-law model, we infer that the observed, non-monotonic formation factor-  
 93 porosity trends in carbonate rocks are the result of an interplay between changing pore  
 94 shape and proportion of resistive material with porosity. When applying the same power-  
 95 law relation to carbonate elastic modeling, we obtain a replacement relationship for the  
 96 empirical  $V_p-V_s$  relations of Pickett (Pickett, 1963) and Castagna (Castagna et al., 1993)  
 97 for wet calcitic rocks, which is derived from first principles and correct in both the high  
 98 and low porosity limit. Finally, a new, first-principles  $V_p/V_s-\phi$  model for porous rocks  
 99 also follows from using this power-law relation in the elastic case.

100 We begin by overviewing the rock physics models used in this paper, before per-  
 101 forming inversions on four electrical (Focke & Munn, 1987) data sets for each rock sam-  
 102 ple’s electrical DEM model inclusion aspect ratio. Parameterizing a power-law relation  
 103 for each data set, we forward model cementation factor and formation factor trends, and  
 104 compare results with Archie’s (Archie, 1942) first law, the Humble (Winsauer et al., 1952)  
 105 equation, and the empirical trends of Focke and Munn (1987). We do not consider the  
 106 double layer effect (Waxman & Smits, 1968) in this study, which can be safely neglected  
 107 in the case of clean carbonates.

108 We then explore whether there are potential benefits of applying this power-law  
 109 relation to carbonate elastic modeling. We perform inversion using three elastic data sets  
 110 (Bakhorji, 2010; Fournier et al., 2011; Verwer, Braaksma, & Kenter, 2008) and param-

111 eterize the corresponding power-law relation with porosity. We forward model bulk and  
 112 shear modulus trends for each data set, as well as  $Vp-Vs$  and  $Vp/Vs-\phi$  trends, and  
 113 compare them with the Pickett (Pickett, 1963) and Castagna (Castagna et al., 1993) em-  
 114 pirical relations. Throughout this paper, we compare the power-law model’s efficiency  
 115 with the typical, single aspect ratio model using the Corrected Akaike Information Cri-  
 116 terion (Hurvich & Tsai, 1989).

## 117 **2 Modeling Approaches**

118 Rock physics trends are generally studied using collections of samples with at least  
 119 one varying characteristic, such as porosity. In this paper, we model the relationships  
 120 between electrical resistivity or elastic moduli and porosity using a number of these col-  
 121 lections, each containing laboratory measurements made on many carbonate core sam-  
 122 ples. We model the data’s effective electrical and elastic properties using the differen-  
 123 tial effective medium (DEM) theory (Berryman, 1992; Mendelson & Cohen, 1982). DEM  
 124 models are constructed by iteratively adding a small volume of ellipsoidal inclusions into  
 125 a background material, homogenizing this composite’s physical properties, and setting  
 126 this new homogenized material as the background material for the subsequent iteration  
 127 until the desired inclusion volume fraction is attained.

### 128 **2.1 Electrical Modeling Background**

129 Mendelson and Cohen (1982) proposed a DEM model to calculate the overall re-  
 130 sistivity of a material consisting of arbitrarily oriented ellipsoidal inclusions in a back-  
 131 ground of conductive material. By making further assumptions - that the inclusions are  
 132 perfectly resistive and the background material is initially water - they derived Archie’s  
 133 (Archie, 1942) first law:

$$F = \phi^{-m}; \tag{1}$$

134 where  $\phi$  is the rock’s pore volume fraction or porosity, and  $m$  is the rock’s cemen-  
 135 tation factor. The rock’s formation factor,  $F$ , can be defined as  $F = \sigma_w/\sigma$  in a fully  
 136 saturated rock, where  $\sigma_w$  is the saturating water’s conductivity and  $\sigma$  is the effective con-  
 137 ductivity. As electrical conductivity and resistivity are mutually reciprocal,  $F$  can be viewed  
 138 as the bulk resistivity of a fluid-flooded rock normalized by the resistivity of the flood-

139 ing fluid. We note equation 1 is missing the coefficient  $a$  presented in the more general  
 140 Humble (Winsauer et al., 1952) equation (e.g., Glover (2016)):

$$F = a\phi^{-m}. \quad (2)$$

141 Salem and Chilingarian (1999) showed by analysis of well log data that  $m$  is strongly  
 142 dependent on the shape of rock grains and pores. This dependence of  $m$  on pore geom-  
 143 etry has been investigated throughout the literature (Glover, 2010; Glover et al., 2000;  
 144 Mendelson & Cohen, 1982; Nigmatullin, Dissado, & Soutougin, 1992). Further to this,  
 145 Focke and Munn (1987) showed cementation factor can be non-constant across a range  
 146 of porosities in carbonates. The derivation of Archie’s first law by Mendelson and Co-  
 147 hen (1982) showed cementation factor  $m$  is a function of grain aspect ratio through de-  
 148 polarization factors  $L_p$ , where  $p \in \{1, 2, 3\}$  refers to the grain’s semi-major axes. De-  
 149 polarization factors relate a background electrical potential field in a homogeneous ma-  
 150 terial to the perturbation potential field caused by the presence of an uncharged, con-  
 151 ducting ellipsoidal grain. Following Mendelson and Cohen (1982), this paper is written  
 152 with the convention  $\sum L_p = 1$ .

153 The expression for cementation factor  $m$  derived by Mendelson and Cohen (1982)  
 154 is:

$$m = \frac{1}{3} \sum_{p=1}^3 \langle (1 - L_p)^{-1} \rangle; \quad (3)$$

155 where angled brackets  $\langle \cdot \rangle$  denote the average over the distribution of grain aspect  
 156 ratios present. Mendelson and Cohen (1982) made the simplification  $L_1 = L$  and  $L_2 =$   
 157  $L_3 = (1 - L)/2$  in equation 3 and averaged over all inclusion orientations for a single  
 158 grain aspect ratio to produce:

$$m = \frac{5 - 3L}{3(1 - L^2)}; \quad (4)$$

159 as was also derived by Gelius and Wang (2008) and T. Han, Clennell, Josh, and  
 160 Pervukhina (2015). Fournier et al. (2011, 2014, 2018) refer to the elastic inclusion as-  
 161 pect ratio,  $\alpha$ , as the “equivalent pore aspect ratio”, or “EPAR”, which we adopt in this

162 paper. In line with this convention, we abbreviate the electrical DEM model aspect ratio  
 163 parameter to “equivalent grain aspect ratio”, or “EGAR”.

## 164 2.2 Elastic Modeling Background

165 The elastic DEM model can be described by the coupled differential equations (Berry-  
 166 man, 1992):

$$(1 - \phi) \frac{d}{d\phi} [K^* (\phi)] = (K_2 - K^* (\phi)) P^{(*2)}; \quad (5)$$

$$(1 - \phi) \frac{d}{d\phi} [\mu^* (\phi)] = (\mu_2 - \mu^* (\phi)) Q^{(*2)}; \quad (6)$$

167 with the initial conditions  $K^*(0) = K_1$  and  $\mu^*(0) = \mu_1$ . Subscript 1 refers to  
 168 background properties, while subscript 2 refers to inclusion properties. Thus, in the case  
 169 of ellipsoidal pores embedded in a mineral background,  $K_1$  and  $\mu_1$  are the mineral bulk  
 170 and shear moduli;  $K_2$  and  $\mu_2$  are the pore fluid bulk and shear moduli;  $K^*$  and  $\mu^*$  are  
 171 the porous rock’s effective bulk and shear moduli; and  $\phi$  is the porosity.

172 Functions  $P$  and  $Q$  (Berryman, 1980) are geometrical functions which are combi-  
 173 nations of select elements of the  $T$  tensor, first put forward by Wu (1966). The  $T$  ten-  
 174 sor relates the strain field in a solitary ellipsoidal inclusion to the strain field applied at  
 175 the boundary of the material in which the inclusion sits. As is the  $T$  tensor, functions  
 176  $P$  and  $Q$  are dependent on the ellipsoidal inclusion’s aspect ratio  $\alpha$ , as well as the elas-  
 177 tic moduli and Poisson’s ratios of the inclusion and background materials. It is evident  
 178 from equations 5 and 6 that the inclusion aspect ratio term  $\alpha$  is present in this formu-  
 179 lation of the elastic DEM model solely through functions  $P$  and  $Q$ . The superscript  $(*2)$   
 180 in equations 5 and 6 indicate  $P$  and  $Q$  are to be calculated assuming the background ma-  
 181 terial in which the inclusion is embedded is in fact the effective medium material itself.

## 182 3 Description of Data

183 We investigate seven public-domain laboratory data sets which come from carbon-  
 184 ate outcrop, surface borehole, and well cores in various global localities. The data have  
 185 varied porosity ranges, diverse pore network architectures, and are approximately monomin-  
 186 eralic. Three of these laboratory data sets have elastic measurements and four have elec-  
 187 trical measurements.



188 We use the carbonate data of Focke and Munn (1987) for our electrical modeling  
 189 tests, as described in Appendix A. We refer to this data as the “FM” data for brevity.  
 190 We use the measurements made on limestones with intergranular porosity; dolostones  
 191 with intergranular porosity; sucrosic dolostones with intercrystalline porosity; and oolitic  
 192 limestones and dolostones with moldic porosity. Sucrosic dolostones are recrystallized  
 193 dolostones with a coarse texture (Dunham, 1962), while moldic pores are fabric-selective  
 194 pores formed by the dissolution of grains (e.g., Choquette and Pray (1970)).

195 Following Focke and Munn (1987), we treat the first three rock types as a single  
 196 data set due to their petrophysical similarities, and model the moldic carbonates as three  
 197 separate data sets, partitioned by their permeabilities:  $0 \leq k < 0.1$  mD;  $0.1 \leq k < 1$   
 198 mD; and  $1 \leq k < 100$  mD. We chose to perform our electrical modeling tests on in-  
 199 tergranular and sucrosic carbonate samples as the pore structure associated with these  
 200 rocks can often be reasonably approximated by an inclusion model. In contrast to this,  
 201 we also chose to perform our electrical model testing on carbonates with moldic poros-  
 202 ity as the assumptions of inclusion models can be highly inappropriate when applied to  
 203 these rocks, which can lead to poor modeling outcomes.

204 We model three of the four public domain elastic data sets investigated by Kittridge  
 205 (2014). These carbonate laboratory data sets are from Verwer et al. (2008), Bakhorji (2010),  
 206 and Fournier et al. (2011), which we will refer to as the “Verwer”, “Bakhorji”, and “Fournier”  
 207 data sets for brevity. Appendix A and Kittridge (2014) present further details on these  
 208 data sets. For elastic modeling, we use only dry measurements made on the subset of  
 209 cores comprised of approximately 100% calcite in the Bakhorji and Fournier data sets,  
 210 and 100% dolomite in the Verwer data set. This experimental design allows us to per-  
 211 form all elastic modeling assuming a two-phase rock, composed of a single-mineral ma-  
 212 trix and air-filled pore space. In doing this, we minimize modeling uncertainties due to  
 213 errors in matrix and fluid compositions.

## 214 **4 Electrical Modeling**

215 To investigate the relationship between EGAR and porosity in electrical DEM mod-  
 216 eling, we inverted for the EGAR of each core sample individually by minimizing the dif-  
 217 ference in the measured and modeled formation factor using equations 1 and 4, assum-  
 218 ing oblate spheroidal inclusions.

219 We displayed the inverted EGARs against measured sample porosity  $\phi$  on a log-  
 220 log scale, as shown in Figure 1. The central observation underpinning our modeling is  
 221 the observed linear trend. We placed a line of best fit through each data set's inverted  
 222 EGARs, with the form:

$$\log \alpha = C + \xi \log \phi, \quad (7)$$

223 where  $C$  and  $\xi$  are the constant and gradient of the line of best fit respectively.

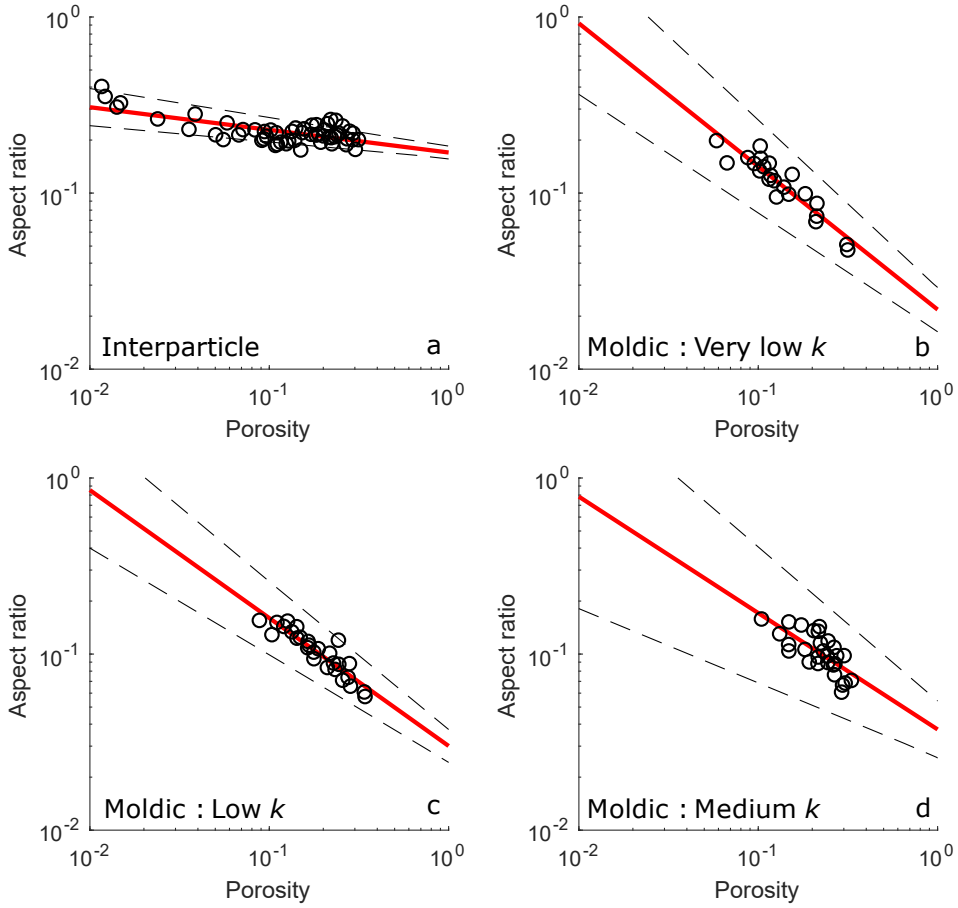


**Figure 1.** Inverted EGARs from the FM data using the electrical DEM model of Mendelson and Cohen (1982). Lines of best fit and their 95% confidence intervals are shown. Subfigures show a) Interparticle porosity; b) Moldic porosity with  $0 \leq k < 0.1$  mD; c) Moldic porosity with  $0.1 \leq k < 1$  mD; and d) Moldic porosity with  $1 \leq k < 100$  mD.

224 Figure 1 also shows each linear fit’s 95% confidence interval on  $C$  and  $\xi$  for each  
 225 data set, calculated from the linear regressions’ covariance matrices.

226 It follows from equation 7 that a best-fitting intercept  $C$  and gradient  $\xi$  become  
 227 parameters  $\{\Gamma, \xi\}$  in the power-law:

$$\alpha = \Gamma\phi^\xi. \quad (8)$$

228 As the inverted EGARs in Figure 1 are not independent of  $\phi$ , we used the solution  
 229 parameters  $\{\Gamma_0, \xi_0\}$  which were obtained from the line of best fit for each data set as the  
 230 starting point in a non-linear inversion to find the true solution parameters  $\{\Gamma^*, \xi^*\}$ . To  
 231 find parameters  $\{\Gamma^*, \xi^*\}$  for each data set, we inverted the nested equations 1, 4, and  
 232 8, 100 times using a fast simulated annealing algorithm (Szu & Hartley, 1987). We then  
 233 chose the optimal solution for each data set to be that which had the lowest  $l_1$ -norm mis-  
 234 fit between the logarithm of the data set’s measured and modeled formation factors. We  
 235 chose this misfit metric for electrical inversion to reduce preferential model fitting at low  
 236 porosities. Initial and final solutions,  $\{\Gamma_0, \xi_0\}$  and  $\{\Gamma^*, \xi^*\}$ , are found in Table 1 for all  
 237 data sets, where we see only small updates in solution parameters between the two in-  
 238 versions.

239 Substituting equation 8 into equations 4 and 1, assuming rock grains are oblate spheroids,  
 240 we obtain a new, explicit expression for formation factor:

$$F = \phi \left[ \frac{1 - \frac{\arcsin\left[\Gamma\phi^\xi\sqrt{\frac{\phi^{-2\xi}}{\Gamma^2} - 1}\right]}{\sqrt{\frac{\phi^{-2\xi}}{\Gamma^2} - 1}}}{\Gamma^2\left(\frac{\phi^{-2\xi}}{\Gamma^2} - 1\right)} \right]^2 \frac{\Gamma^2\phi^{2\xi}\left(\sqrt{\frac{\phi^{-2\xi}}{\Gamma^2} - 1} - \arcsin\left[\Gamma\phi^\xi\sqrt{\frac{\phi^{-2\xi}}{\Gamma^2} - 1}\right]\right)^2}{(\Gamma^2\phi^{2\xi} - 1)^3} + 1 \quad (9)$$

241 We forward-modeled cementation factor and formation factor trends for all elec-  
 242 trical data sets using parameters  $\{\Gamma^*, \xi^*\}$  and equation 9, as shown in Figures 2 and 3  
 243 respectively. The set of green curves display the power-law model, which fits both the  
 244 formation and cementation factor data more accurately than the best fitting Archie’s law,  
 245 shown in dashed red. They also approximate the empirical models of Focke and Munn  
 246 (1987), displayed with dotted black lines. The Humble equation may provide a suitable  
 247 fit to the data in Figure 3, however it is incorrect in the limit when  $\phi \rightarrow 1$ . As  $\xi < 0$

248 for all four modeled data sets, and as grains are assumed to be oblate spheroids, the power-  
 249 law model is only valid on porosities above that where  $\alpha = 1$ . When  $\alpha = 1$ ,  $m = 3/2$   
 250 and the power-law model reduces to the model of Sen, Scala, and Cohen (1981), indi-  
 251 cated by an empty black square in Figure 2.

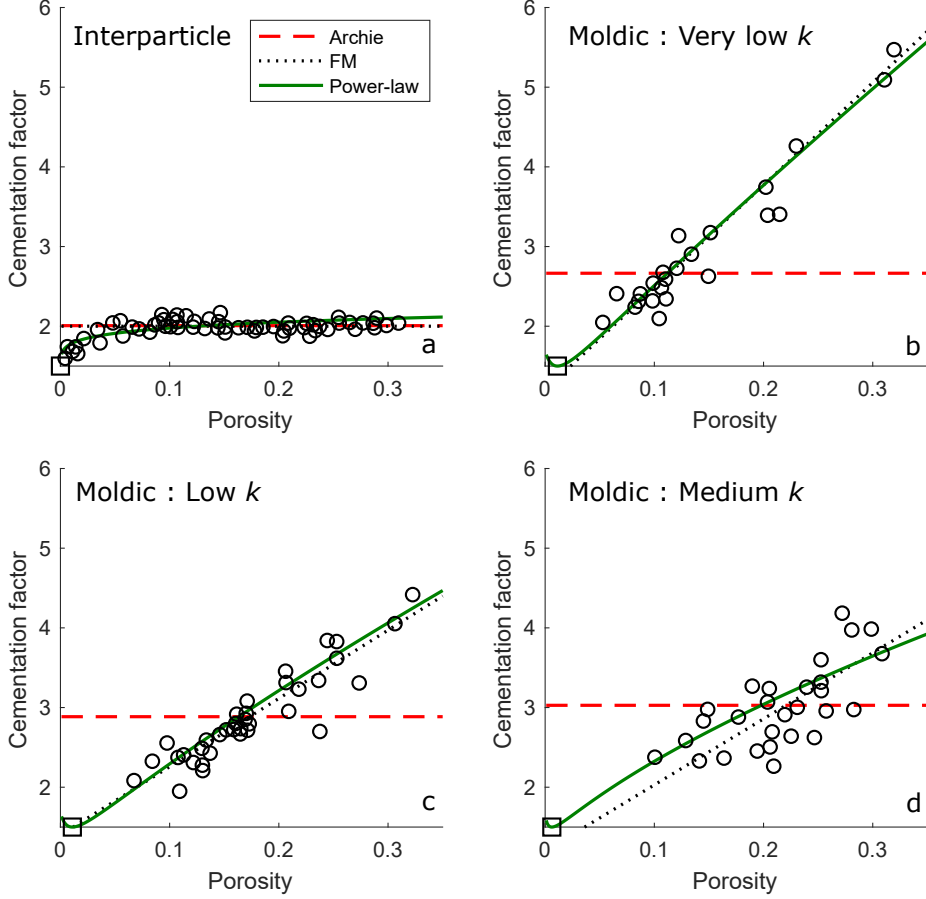


**Figure 2.** Forward-modeled cementation factor for the FM data using the power-law DEM model (solid), Archie’s first law (dashed), and Focke and Munn’s empirical relationships (dotted). The lower bound of the power-law model’s valid porosity range is also shown (square). Subfigures show a) Interparticle porosity; b) Moldic porosity with  $0 \leq k < 0.1$  mD; c) Moldic porosity with  $0.1 \leq k < 1$  mD; and d) Moldic porosity with  $1 \leq k < 100$  mD.

252 Table 1 summarizes the electrical inversion results, with a 50% to 85% improve-  
 253 ment in the residual sum of squares (RSS) error on Archie’s law across all FM data sets.  
 254 To quantitatively establish the preferred model for each data set, we use the Corrected  
 255 Akaike Information Criterion (Hurvich & Tsai, 1989), as reviewed in Appendix B. All

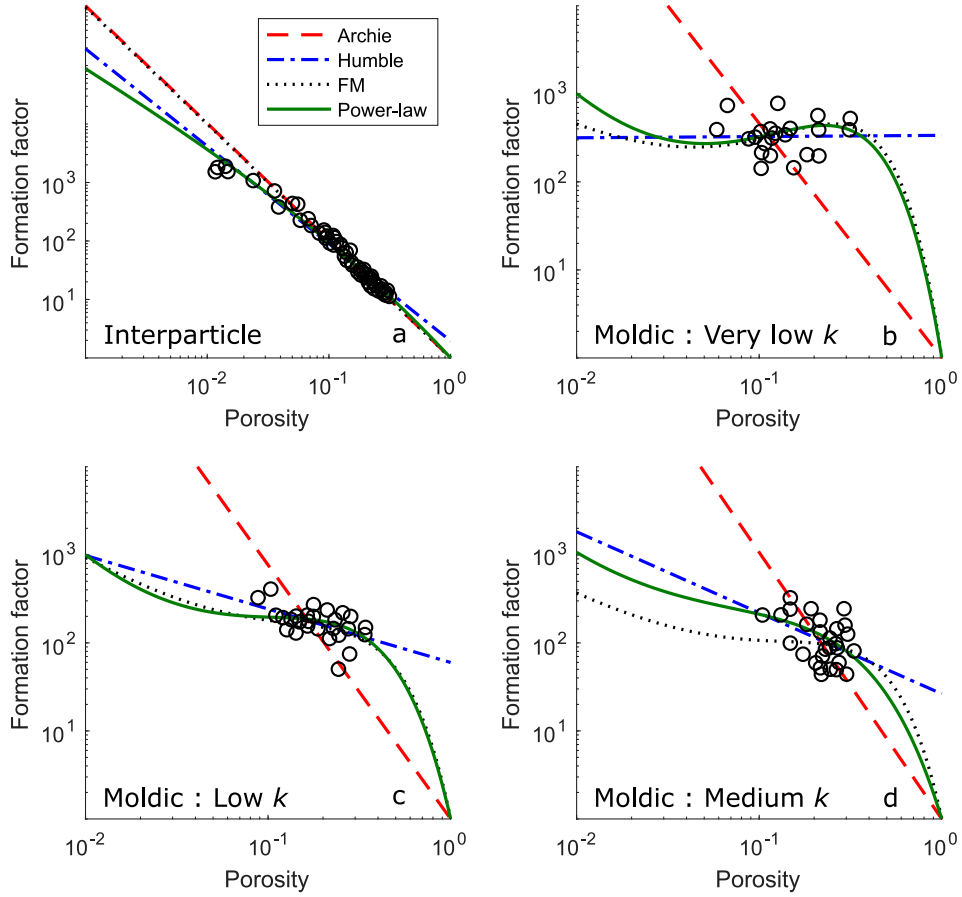


**Figure 3.** Forward-modeled formation factor for the FM data using the power-law DEM model (solid), Archie's first law (dashed), the Humble equation (dot-dashed), and Focke and Munn's empirical relationships (dotted). Subfigures show a) Interparticle porosity; b) Moldic porosity with  $0 \leq k < 0.1$  mD; c) Moldic porosity with  $0.1 \leq k < 1$  mD; and d) Moldic porosity with  $1 \leq k < 100$  mD.

256 modeling log-relative likelihoods were much greater than 10, meaning there is compelling  
 257 evidence supporting the use of the power-law model over Archie’s law on all electrical  
 258 data sets.

259 There is a theoretical possibility for certain model parameters that aspect ratio can  
 260 be greater than unity, which would be inconsistent with the modeling assumption of oblate  
 261 spheroids. As such, we show the range of porosities where the power-law model is valid  
 262 in Table 1.

263 The points of inflexion and turning points in the power-law forward-modeled for-  
 264 mation factor trends are not present in Archie’s law but are key features in the empir-  
 265 ical models of Focke and Munn (1987). We infer these special points are due to the com-  
 266 peting effects of inclusion geometry and pore volume fraction on a porous rock’s over-  
 267 all resistivity. A porous rock’s resistivity decreases with increasing porosity due to a re-  
 268 duction in the amount of insulating material. The resistivity of a rock comprised of el-  
 269 lipsoidal grains, however, increases with grain eccentricity, as shown by Mendelson and  
 270 Cohen (1982). These two effects compete in the FM data, where inclusions become more  
 271 eccentric with increasing porosity, leading to the non-monotonic formation factor trends  
 272 observed by Focke and Munn (1987) and in Figure 3.

## 273 **5 Elastic Modeling**

274 We have seen how including a power-law between equivalent grain aspect ratio and  
 275 porosity in an electrical DEM model can lead to effective modeling of rocks with com-  
 276 plex pore geometries. Given this result, we now examine if a power-law between pore  
 277 aspect ratio and porosity in an elastic DEM model is beneficial for the elastic modeling  
 278 of rocks with complex pore geometries.

### 279 **5.1 Bulk Modulus Modeling**

280 To investigate the relationship between bulk modulus EPAR and porosity in elas-  
 281 tic DEM modeling, we first calculated a measured effective bulk and shear modulus for  
 282 each core of the three elastic data sets using the laboratory-measured  $P$ - and  $S$ -wave ve-  
 283 locities, and bulk density. With known mineralogy and porosity from experimental data,  
 284 and mineral moduli shown in Table 2, we inverted for each sample’s bulk modulus EPAR  
 285 by minimizing the difference between measured and modeled bulk modulus using equa-

**Table 1.** Electrical modeling results.

Electrical inversion (Pore type)	$n$	$\{\Gamma_0, \xi_0\}$	$\{\Gamma^*, \xi^*\}$	$m_{Archie}^*$	$a_{Humble}^*$	$m_{Humble}^*$	Valid porosities	% RSS decrease on Archie's Law	Log-relative likelihood $\Delta AIC_C$
Focke and Munn (1987) (Interparticle)	55	{0.170, -0.129}	{0.173, -0.122}	2.01	1.97	1.67	$\phi > 10^{-6}$	68.8	61.8
Focke and Munn (1987) (Moldic: Very low $k$ )	22	{0.022, -0.813}	{0.018, -0.895}	2.67	338	-0.01	$\phi > 0.011$	85.6	40.0
Focke and Munn (1987) (Moldic: Low $k$ )	27	{0.030, -0.727}	{0.026, -0.808}	2.89	59.8	0.61	$\phi > 0.011$	83.5	46.1
Focke and Munn (1987) (Moldic: Medium $k$ )	28	{0.037, -0.661}	{0.036, -0.650}	3.03	26.3	0.92	$\phi > 0.006$	52.5	18.3

286 tions 5 and 6. As was done in the electrical case (Section 4), we then calculated initial  
 287 model parameters  $\{\Gamma_0, \xi_0\}$  for each data set by fitting a line of best fit through the cross-  
 288 plot of inverted EPARs and measured porosities on a log-log scale. Following this, we  
 289 inverted equations 5, 6, and 8 for  $\{\Gamma^*, \xi^*\}$  100 times using a fast simulated annealing al-  
 290 gorithm, choosing the final solution parameters as those which led to the lowest misfit  
 291 out of all 100 solutions, as was done in the electrical modeling case. Unlike the inver-  
 292 sion for electrical model parameters, the minimized objective function in the inversion  
 293 for bulk modulus  $\{\Gamma^*, \xi^*\}$  was the  $l_2$ -distance between the measured and modeled bulk  
 294 moduli for each data set.

295 Figure 4 shows the inverted bulk modulus EPARs for each sample, as well as the  
 296 line of best fit used to calculate  $\{\Gamma_0, \xi_0\}$  for each elastic data set, and the 95% confidence  
 297 intervals associated with these fits. Parameters  $\{\Gamma_0, \xi_0\}$  and  $\{\Gamma^*, \xi^*\}$  are found in Ta-  
 298 ble 3 for all elastic data sets, where we see only small updates in solution parameters be-  
 299 tween the two inversions.

300 We forward-modeled best-fitting  $\phi - K$  trends using equations 5, 6, and 8 given  
 301 the optimal parameters  $\{\Gamma^*, \xi^*\}$ . We also calculated the best fitting EPAR which is con-  
 302 stant in porosity,  $\alpha_{DEM}^*$ , for each data set and forward-modeled the corresponding Single-  
 303  $\alpha$  DEM  $\phi - K$  trends for comparison (Figure 5). Figures 5a and 5b show the power-  
 304 law DEM model appears more accurate than Single- $\alpha$  DEM, particularly at low porosi-  
 305 ties. In fact, the percentage decrease in elastic modeling RSS error by using the power-  
 306 law DEM model over Single- $\alpha$  DEM model is seen in Table 3 to be over 60% in the Bakhorji  
 307 data. Figure 5c is an example of the power-law model collapsing to a Single- $\alpha$  DEM  
 308 model, with  $\xi^* \approx 0$ , and hence  $\Gamma^* \approx \alpha_{DEM}^*$  (Table 3).

309 Table 3 shows the log-relative likelihood ( $\Delta AIC_C$ ) for all bulk modulus elastic mod-  
 310 eling comparisons, which is greater than ten for the Bakhorji and Fournier data sets. Fol-  
 311 lowing the model selection convention described in Appendix B, we conclude there is com-  
 312 pelling evidence for the use of the power-law model in these cases. In modeling the Ver-  
 313 wer data, when the power-law model approximates the special case of a Single- $\alpha$  DEM  
 314 model, both models generate a similar  $\phi - K$  trend (Figure 5c) but the Single- $\alpha$  DEM  
 315 model has fewer parameters. The corresponding  $\Delta AIC_C$  is -1.9, which supports the use  
 316 of the Single- $\alpha$  model. We also show the range of porosities where the model is valid in  
 317 Table 3, noting this is effectively all porosities on all elastic data sets.



**Table 2.** Elastic parameters used in modeling.

Constituent	Bulk Modulus (Pa)	Shear Modulus (Pa)	Density (kg/m <sup>3</sup> )	References
Calcite	$76.8 \times 10^9$	$32.0 \times 10^9$	$2.71 \times 10^3$	Simmons (1965)
Dolomite	$94.9 \times 10^9$	$45.0 \times 10^9$	$2.87 \times 10^3$	Humbert and Plicque (1972)
Quartz	$36.6 \times 10^9$	$45.0 \times 10^9$	-	T. Han, Best, MacGregor, Sothcott, and Minshull (2011) Mavko, Mukerji, and Dvorkin (2009)
Clay	$20.9 \times 10^9$	$6.85 \times 10^9$	-	Mavko et al. (2009); Tosaya (1982); T. Han et al. (2011)
Water	$2.3 \times 10^9$	0	-	T. Han et al. (2011)
Air	$1.01 \times 10^5$	0	1.29	Mavko et al. (2009)

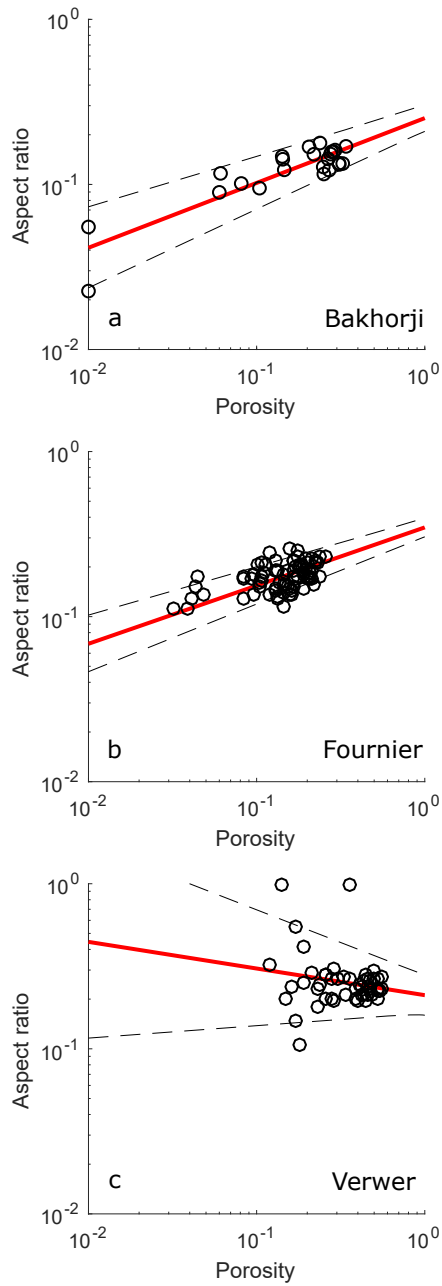


**Figure 4.** Inverted EPARs (circles) from bulk modulus data. Lines of best fit (solid red) and their 95% confidence intervals (dashed black) are shown. Subfigures show a) the Bakhorji data set; b) the Fournier data set; and c) the Verwer data set.

**Table 3.** Elastic modeling results.

Elastic inversion	$n$	$\{\Gamma_0, \xi_0\}$	$\{\Gamma^*, \xi^*\}$	$\alpha_{DEM}^*$	Valid porosities	% RSS decrease on Single- $\alpha$ DEM	Log-relative likelihood $\Delta AIC_C$
Bakhorji (2010) <i>K</i> -Inversion	24	{0.252, 0.393}	{0.257, 0.387}	0.13	All $\phi$	60.5	19.7
Bakhorji (2010) $\mu$ -Inversion	24	{0.273, 0.561}	{0.257, 0.521}	0.12	All $\phi$	48.8	13.6
Fournier et al. (2011) <i>K</i> -Inversion	80	{0.347, 0.352}	{0.277, 0.238}	0.17	All $\phi$	22.1	17.9
Fournier et al. (2011) $\mu$ -Inversion	80	{0.379, 0.562}	{0.296, 0.439}	0.13	All $\phi$	41.6	40.8
Verwer et al. (2008) <i>K</i> -Inversion	51	{0.211, -0.116}	{0.231, -0.046}	0.25	$\phi > 10^{-13}$	0.7	-1.9
Verwer et al. (2008) $\mu$ -Inversion	51	{0.185, 0.024}	{0.204, 0.140}	0.17	All $\phi$	4.3	0.0
Combined calcites <i>K</i> -Inversion	104	{0.312, 0.345}	{0.264, 0.246}	0.17	All $\phi$	17.0	17.3
Combined calcites $\mu$ -inversion	104	{0.338, 0.542}	{0.249, 0.381}	0.13	All $\phi$	26.3	29.6

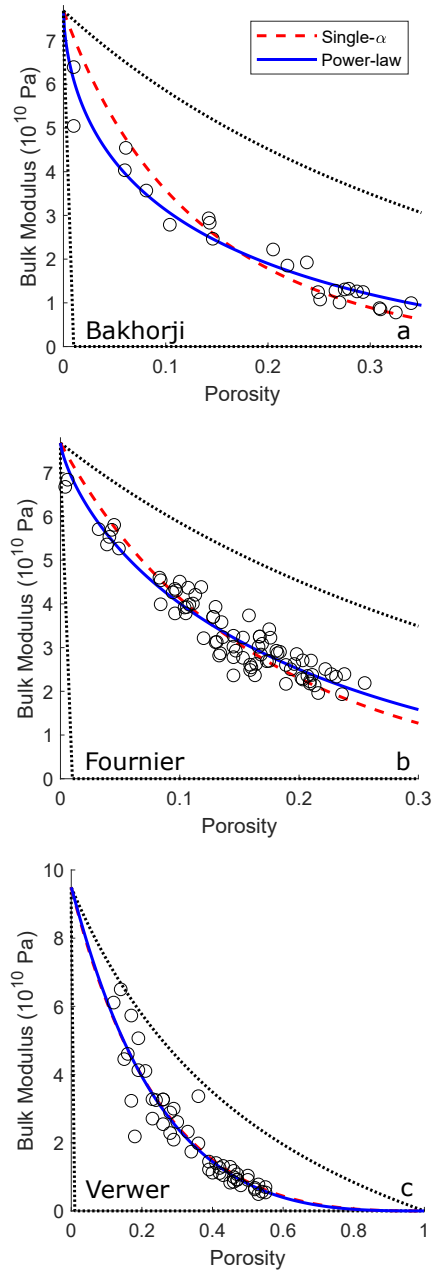


**Figure 5.** Forward-modeled bulk modulus from the power-law DEM (solid blue) and optimal Single- $\alpha$  DEM (dashed red) models, as well as measured data (circles), and the Hashin-Shtrikman bounds (dotted black bounding curves). Subfigures show a) the Bakhorji data set; b) the Fournier data set; and c) the Verwer data set. Notice the power-law and Single- $\alpha$  DEM trends are almost identical in the Verwer data.

## 318 5.2 Shear Modulus and $V_p$ - $V_s$ Modeling

319 A shortcoming of elastic inclusion modeling is the practical inability to model both  
 320 a rock's bulk and shear modulus using the same EPAR. This is observed by Fournier et  
 321 al. (2011, 2014, 2018), and is usually attributed to the presence of asperities in pores.  
 322 In fact, Fournier et al. (2014, 2018) investigate the relationship between bulk and shear  
 323 modulus EPARs and exploit this relationship to effectively characterize different litholo-  
 324 gies. In this section, we first mathematically relate the bulk and shear modulus EPARs  
 325 of a rock before deriving  $V_p$ - $V_s$  and  $V_p/V_s$ - $\phi$  models based on elastic DEM theory and  
 326 the proposed power-law relationship.

327 We denote the rock's porosity-dependent bulk and shear modulus EPARs by  $\alpha_K(\phi)$   
 328 and  $\alpha_\mu(\phi)$  respectively. Similarly,  $\{\Gamma_K, \xi_K\}$  and  $\{\Gamma_\mu, \xi_\mu\}$  are their respective power-law  
 329 model parameters.

330 We inverted for the shear modulus parameters  $\{\Gamma_\mu, \xi_\mu\}$  of the three elastic data  
 331 sets by the same method as bulk modulus inversion but minimizing shear modulus mis-  
 332 fit. Figure 6 shows the parameterized linear  $\phi - \alpha$  trends on a log-log plot after shear  
 333 modulus inversion.

334 Initial and final shear modulus parameters are displayed in Table 3 and are distin-  
 335 guished by the subscript "0" and superscript "\*" respectively.

336 Figure 7 shows that forward-modeling  $\phi - \mu$  trends seems to generate more ac-  
 337 curate fits over standard, Single- $\alpha$  DEM methods, in the Bakhorji and Fournier data sets.  
 338 Comparing the proposed power-law model and the best-fitting Single- $\alpha$  DEM model in  
 339 terms of log-relative likelihoods, there is compelling evidence that the power-law model  
 340 is the best model for use on the Bakhorji and Fournier shear modulus data, with  $\Delta AIC_C >$   
 341 10 (Table 3). It is approximately equally likely the power-law and Single- $\alpha$  DEM mod-  
 342 els are the best model by the  $AIC_C$  metric for the Verwer data set as  $\Delta AIC_C = 0.0$ .

343 From equation 8, the ratio of  $\alpha_K(\phi)$  and  $\alpha_\mu(\phi)$  is:

$$\alpha_\mu(\phi) = \frac{\Gamma_\mu}{\Gamma_K} \phi^{\bar{\xi}} \alpha_K(\phi); \quad (10)$$

344 where  $\bar{\xi} = \xi_\mu - \xi_K$ .

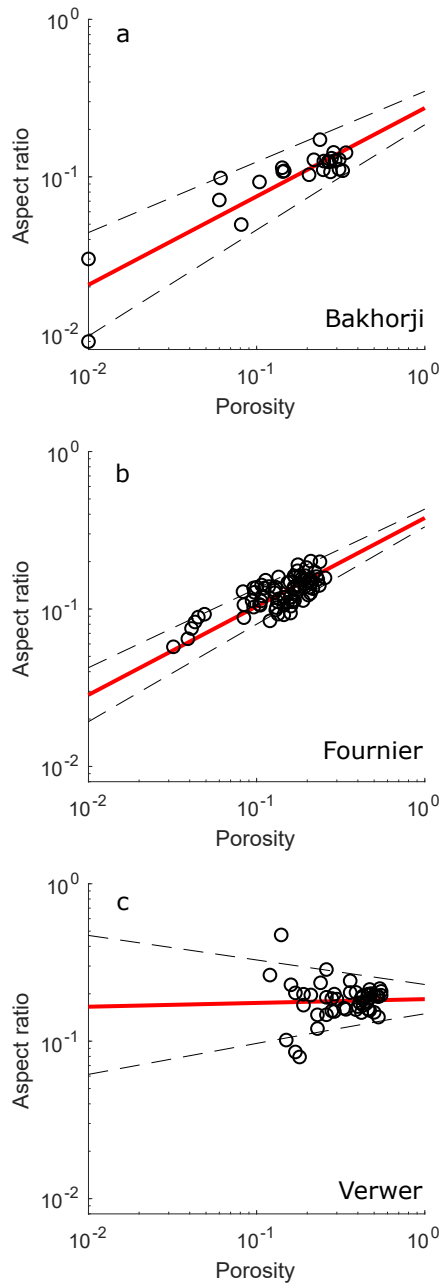


**Figure 6.** Inverted EPARs (circles) from shear modulus data. Lines of best fit (solid red) and their 95% confidence intervals (dashed black) are shown. Subfigures show a) the Bakhorji data set; b) the Fournier data set; and c) the Verwer data set.

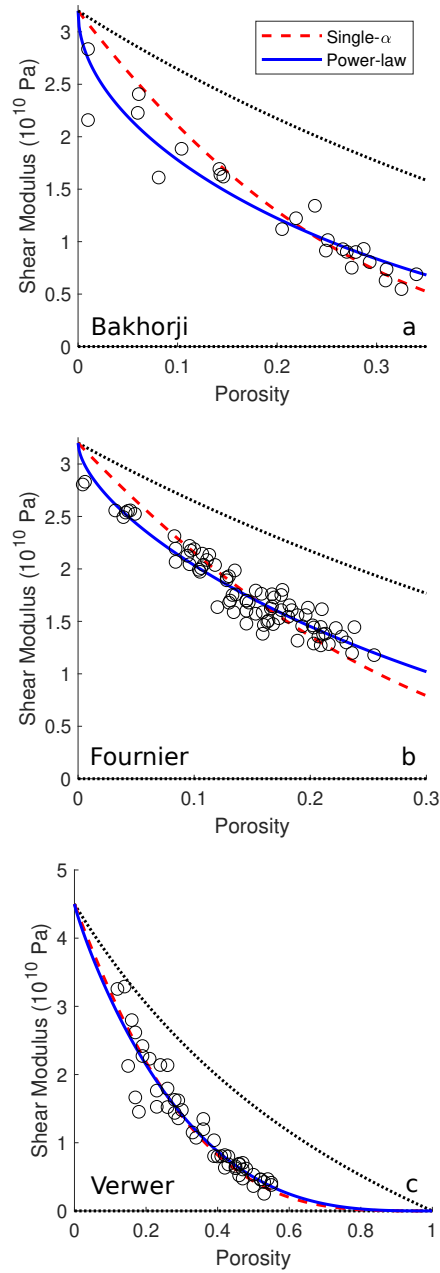


**Figure 7.** Forward-modeled shear modulus from the power-law DEM (solid blue) and optimal Single- $\alpha$  DEM (dashed red) models, as well as measured data (circles), and the Hashin-Shtrikman bounds (dotted black bounding curves). Subfigures show a) the Bakhorji data set; b) the Fournier data set; and c) the Verwer data set. Notice the power-law and Single- $\alpha$  DEM trends are almost identical in the Verwer data.

345 In Table 3, we observe  $\Gamma_\mu^*$  and  $\Gamma_K^*$  are similar for the Bakhorji and Fournier data  
 346 sets, implying  $\alpha_K$  and  $\alpha_\mu$  are similar in the high porosity limit. Given the observed sim-  
 347 ilarity of  $\Gamma_\mu^*$  and  $\Gamma_K^*$  in the Fournier and Bakhorji data sets, we modeled a calcite  $V_p/V_s$ -  
 348  $\phi$  relationship using the approximation:

$$\alpha_\mu(\phi) \approx \phi^{\bar{\xi}} \alpha_K(\phi) . \quad (11)$$

349 Thus we see parameter  $\bar{\xi}$  quantifies the difference in how bulk and shear modulus  
 350 EPARs change with porosity.

351 Figure 8 shows the inverted bulk and shear modulus EPARs for each calcitic core  
 352 sample, taken from the Bakhorji and Fournier data sets, and the forward-modeled  $\alpha_\mu$ -  
 353  $\alpha_K$  trend for calcites. We forward-modeled effective bulk and shear modulus trends us-  
 354 ing the elastic DEM model (equations 5 and 6) and equation 11. Following this, we forward-  
 355 modeled a  $V_p$ - $V_s$  trend for dry calcitic rocks using densities from Table 2. Water-saturating  
 356 the modeled dry  $V_p$ - $V_s$  trend using Gassmann (1951) fluid substitution, we compare the  
 357 model's behavior with the empirical relations of Pickett (1963) and Castagna et al. (1993)  
 358 in Figure 8 for wet calcite. The power-law DEM model evidently approximates the em-  
 359 pirical models in the range of the data, while having the added benefits of being correct  
 360 in the high and low porosity limits and being based on first principles.

361 Figure 8 also shows the forward-modeled  $V_p/V_s$ - $\phi$  trend calculated for dry calcite  
 362 using the  $V_p$  and  $V_s$  trends obtained through equation 11. The laboratory measured data  
 363 are shown and generally agree with this analytically derived  $V_p/V_s$ - $\phi$  trend.

## 364 6 Discussion

365 We have presented a modified DEM model which fits 7 public-domain electrical and  
 366 elastic data sets more accurately than the typical DEM modeling approach. This im-  
 367 proved fitting, however, is at the expense of an extra model parameter, which we have  
 368 justified using log-relative likelihood analysis. Model parameters  $\xi$  and  $\Gamma$  both have a  
 369 physical interpretation. Parameter  $\xi$  signifies the rate at which EPAR or EGAR changes  
 370 with porosity. It follows that  $\xi$  may be an indicator of how a rock is affected by the phys-  
 371 ical processes which alter pore geometry such as diagenesis. Parameter  $\Gamma$  indicates the



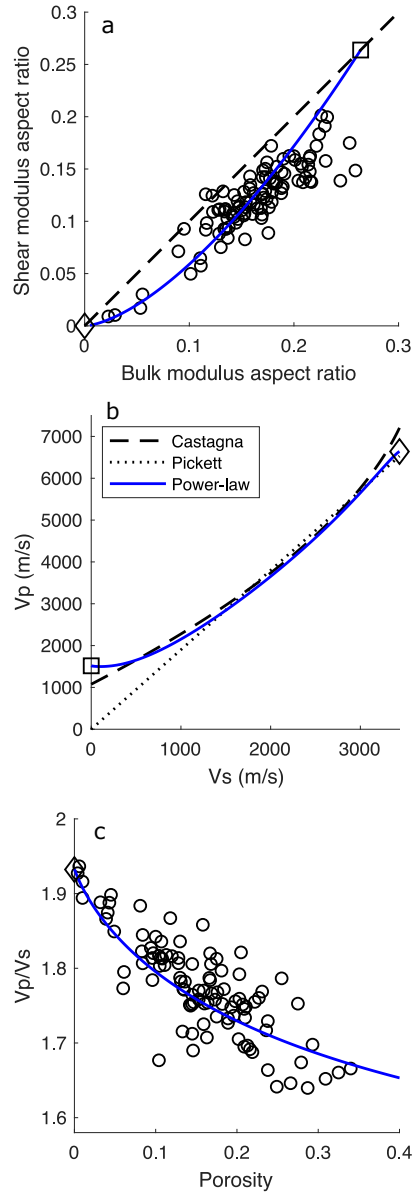


**Figure 8.**  $V_p$ - $V_s$  modeling of the combined Bakhorji and Fournier calcitic data sets. Diamond markers denote 100% calcite, while squares denote 100% fluid. a) The  $\alpha_\mu$ - $\alpha_K$  trend (solid blue) and inverted EPARs from dry laboratory measurements (circles) are shown with a dashed 1:1 line for reference. b) The Gassmann-wetted power-law DEM  $V_p$ - $V_s$  trend (solid blue) is shown with the Castagna et al. (1993) (dashed black) and Pickett (1963) (dotted black) empirical relations for wet calcite. c) The dry power-law DEM  $V_p/V_s$ - $\phi$  trend (solid blue) is shown with dry laboratory measurements (circles).

372 limiting EPAR or EGAR when  $\phi \rightarrow 1$ , and therefore indicates the expected stiffness  
 373 of a rock at high porosities.

374 We have selected data with highly-constrained mineralogy and fluid content to min-  
 375 imize errors in EPAR or EGAR inversion. The fluid content and hence its electrical re-  
 376 sistivity is largely unknown in the experiments of Focke and Munn (1987). However, Focke  
 377 and Munn (1987) note that formation factor does not appear to be affected by the brine's  
 378 resistivity in clean carbonates. The extension of the work in this paper to multiminer-  
 379 alic and multifluid rocks may have larger modeling errors as additional, mixing models  
 380 must also be used. The proposed power-law electrical model is not designed to account  
 381 for the double-layer effect (Waxman & Smits, 1968) as all solid phases are assumed to  
 382 be insulating.

383 Archie's (Archie, 1942) contribution was to show that resistivity of fully saturated  
 384 sandstones followed a simple law given by equation 1, but unfortunately it became clear  
 385 that carbonates showed more complex relationships. Several authors tried to address this  
 386 variability by allowing cementation factor to vary with porosity in Archie's law, deduc-  
 387 ing values that varied from 1 to greater than 4 (Focke & Munn, 1987; Verwer, Eberli,  
 388 & Weger, 2011). Although undeniably useful, these porosity varying forms can be read  
 389 as definitions of cementation factor; any combination of formation factor and porosity  
 390 can be modeled with a suitable choice of the value  $m$ . Our goal in this paper was to link  
 391 this implicit cementation factor-porosity relationship directly to details of the pore-structure,  
 392 leading the way to making the formulation predictive.

393 The presented power-law model has the same number of model parameters as the  
 394 critical porosity model of Mukerji, Berryman, Mavko, and Berge (1995). This power-law  
 395 model can act as an approximate critical porosity model when  $\xi < 0$ , as well as the Single-  
 396  $\alpha$  DEM model when  $\xi = 0$ . The power-law model's form when  $\xi > 0$  cannot be ap-  
 397 proximated by the typical critical porosity model, however, which may make the power-  
 398 law model preferable in the case of an unknown critical porosity.

399 The sign of parameter  $\xi^*$  is positive in the elastic case, and negative in the elec-  
 400 trical case. This is due to the elastic model being constructed with inclusions of fluid be-  
 401 ing embedded into a background of matrix, while the electrical model is constructed with  
 402 inclusions of grain material being embedded into a background of fluid.

403 A major drawback of modeling with the Humble equation is that it is non-physical  
 404 in the high-porosity limit. The proposed electrical power-law DEM model addresses this  
 405 issue. It models carbonate data with comparable accuracy to the Humble equation (Fig-  
 406 ure 3) and uses the same number of model parameters, but is correct when  $\phi \rightarrow 1$ , like  
 407 Archie’s first law.

408 Our claim of a non-constant relationship between porosity and EPAR may seem  
 409 to contrast with that of Fournier et al. (2018), who conclude EPAR is constant in min-  
 410 eralogy and porosity for carbonates with a given dominant pore type. Fournier et al. (2018),  
 411 however, do observe a change in EPAR with porosity for a given carbonate facies (e.g.,  
 412 in spherulites from offshore Brazil). Further, Fournier et al. (2018) show diagenetic al-  
 413 teration in carbonates, such as vug-forming dissolution, leads to altered EPARs. Our find-  
 414 ings may therefore be consistent with the foundational works of Fournier et al. (2011,  
 415 2014, 2018) if our investigated samples are diagenetically altered or differ in dominant  
 416 pore type across different porosities.

## 417 **7 Conclusion**

418 We argue that introducing a power-law relationship between porosity and aspect  
 419 ratio improves the efficiency of modeling the variation of electrical properties with poros-  
 420 ity, and also observe benefits when using this power-law relation in elastic modeling. Much  
 421 interpretation of resistivity or velocity in terms of porosity depends on a small number  
 422 of empirical relationships, which are known to break down in many important cases. Our  
 423 power-law leads to alternative relationships which are derived from first principles, re-  
 424 produce the empirical relations over much of the porosity range, and are exactly correct  
 425 in the high and low porosity limits. This provides a basis for extrapolating the empir-  
 426 ical relationship to different geological conditions, as well as an alternative in situations  
 427 where the empirical models are known to fail, as is the case with Archie’s first law in many  
 428 carbonates. Use of the power-law model to link electrical and elastic properties would  
 429 require a data set with both measurements, but we hope the proposed models are a step  
 430 towards multiphysics modeling from first principles.

## 431 **A Data review**

432 The resistivity data of Focke and Munn (1987) are laboratory resistivity measure-  
 433 ments made on reservoirs core from offshore Qatar. No pore fluid conductivity or salin-

434 ity measurements were provided in the original publication of Focke and Munn (1987).  
 435 Rather, it was noted that the experimental pore fluid simulated formation water for all  
 436 data sets. Similarly, mineralogical measurements were not available, but it was noted that  
 437 most plugs were made of clean carbonates. Having no tabulated data, we digitized the  
 438 data manually.

439 We studied only subsets of the Verwer (Verwer et al., 2008), Fournier (Fournier et  
 440 al., 2011), and Bakhorji (Bakhorji, 2010) elastic data sets to minimize the influence of  
 441 confounding factors on our modeling results. Table A.1, adapted from Kittridge (2014),  
 442 shows data set details. We selected only dry measurements for elastic modeling made  
 443 on approximately monomineralic samples.

444 We studied the 51-sample subset from the Verwer data set which contained poros-  
 445 ity, dry  $V_p$ , dry  $V_s$ , dry bulk density measurements, and had 100% dolomite composi-  
 446 tion to the nearest integer by XRD analysis. We modeled this data assuming 100% dolomite  
 447 mineralogy using the elastic parameters shown in Table 3. We used the dry core mea-  
 448 surements of the Bakhorji data set at 20 MPa confining pressure from the loading stage  
 449 of the loading-then-unloading experimental regime, as was done by Kittridge (2014). We  
 450 studied the 24-sample subset from this Saudi-D reservoir data which contained at least  
 451 90% calcite by volume. The median composition of these samples was 99% calcite, so  
 452 we modeled the data set using a 100% calcite mineralogy with the elastic parameters shown  
 453 in Table 3. We studied the dry, elastic measurements of the Fournier data set made at  
 454 20 MPa confining pressure on all 80 calcitic cores and modeled this data set with a 100%  
 455 calcite mineralogy.

## 456 **B Corrected Akaike Information Criterion**

457 The Akaike Information Criterion (AIC) (Akaike, 1973) is a model selection cri-  
 458 terion based in Information theory which estimates the most likely amount of informa-  
 459 tion lost when approximating measured data generated by a true, unknown model, with  
 460 a candidate, fitted model. The AIC does this by estimating the fitted model’s expected  
 461 Kullback-Leibler divergence (Kullback & Leibler, 1951) from the true, unknown model  
 462 which generates the measured data. Hurvich and Tsai (1989) formulate the AIC as:

$$AIC = n (\log \hat{s}^2 + 1) + 2 (p + 1) ; \quad (B.1)$$

**Table A.1.** Summary of elastic core data sets analyzed (Adapted from Kittridge (2014)).

Source	Location	Type	#Spl	Lab velocity	Description	Additional descriptor(s)
Verwer <i>et al.</i> (2008)	Cap Blanc of the Lluçmàjor Platform, Mallorca	Outcrop and surface borehole (3)	250	Wet (deaired brine 3% NaCl) and dry; Peff 10 MPa; Ppore 0.1 MPa; 1 MHz	Miocene; low- and high- Mg calcite, dolomite, aragonite. Mostly dolomitic	XRD, petrography, texture (granular, crystalline)
Bakhorji (2010)	Arab-D reservoir (Saudi Arabia) with seven wells	Wells	37	Wet and dry; Pconf 5-25 MPa (increasing, decreasing stress); ~1 MHz	Limestone or Dolomite (<1% noncarbonate)	Samples characterized as macro, micro, dual porosity. Petrography, SEM, mercury porosimetry
Fournier <i>et al.</i> (2011)	Four outcrop locations South East France	Outcrop	80	Dry; Pconf 2.5, 5, 10, 20, and 40 MPa; Ppore 0.1 MPa; 1 MHz	Lower Cretaceous platform; microporous limestone	All grainstone texture, absence of intergranular, intercrystalline, or moldic porosity

463 where  $n$  is the number of samples,  $p$  is the number of model parameters, and  $\hat{s}$  is  
 464 the maximum likelihood estimate of the measured data's variance.

465 The  $AIC$  is biased in the case of small  $n$ , where it tends to favor models with larger  
 466  $p$  (Hurvich & Tsai, 1989). As our data sets are relatively small, we compare models us-  
 467 ing the Corrected Akaike Information Criterion ( $AIC_C$ ) (Hurvich & Tsai, 1989), which  
 468 is more accurate in small  $n$ . Hurvich and Tsai (1989) derive the  $AIC_C$  as:

$$AIC_C = AIC + \frac{2(p+1)(p+2)}{n-p-2}. \quad (\text{B.2})$$

469 We see the second, additive term on the right-hand side of equation B.2 goes to  
 470 0 when  $n \gg p$ , approximating the  $AIC$ , and is non-negligible when  $p$  and  $n$  are com-  
 471 parable. The difference,  $\Delta AIC_C$ , in the  $AIC_C$  values of a reference and candidate model  
 472 indicates the evidence for using one model over the other. It is the logarithm of the rel-  
 473 ative likelihood of the two models, conditional on the model parameters and residuals  
 474 from the data (Burnham & Anderson, 2002). We thus refer to the  $\Delta AIC_C$  as the *log-*  
 475 *relative likelihood* throughout this paper.

476 For example, we can compare the two-parameter, power-law (superscript “PL”) model  
 477 with the best single-parameter (superscript “DEM”) model using the  $\Delta AIC_C$ , which we  
 478 define as:

$$\Delta AIC_C = AIC_C^{\text{DEM}} - AIC_C^{\text{PL}}. \quad (\text{B.3})$$

479 The value of  $\Delta AIC_C$  here indicates the evidence that the proposed power-law model  
 480 is more likely to be more efficient than the single-aspect ratio (“Single- $\alpha$ ”) DEM model.  
 481 Burnham and Anderson (2002, 2004) provide useful rules of thumb for the interpreting  
 482 the log-relative likelihood of competing models, analogous to the popular advice of Raftery  
 483 (1996) or Jeffreys (1998) in the Bayesian model selection literature. Applied specifically  
 484 to our formulation of  $\Delta AIC_C$ , these guidelines suggest if  $\Delta AIC_C > 0$ , the power-law  
 485 model is considered to be the best model, however if:

- 486 1.  $0 < \Delta AIC_C < 2$  : Single- $\alpha$  DEM has substantial evidence as best model.
- 487 2.  $4 < \Delta AIC_C < 7$  : Single- $\alpha$  DEM has considerably less evidence.
- 488 3.  $\Delta AIC_C > 10$  : Single- $\alpha$  DEM has essentially no evidence.

489 We reframe these guidelines to focus on the power-law model, proposing and dis-  
 490 cussing results in terms of the complimentary case:

491 4.  $\Delta AIC_C > 10$  : Power-law model has compelling evidence as best model.

492 When  $\Delta AIC_C < 0$ , Single- $\alpha$  DEM is accepted as the best model and the mag-  
 493 nitude of the log-relative likelihood is used to measure the evidence that the power-law  
 494 model is the best model under Burnham and Anderson's guidelines.

## 495 Acknowledgments

496 The authors would like to thank Petrobras and Shell for their sponsorship of the Inter-  
 497 national Center for Carbonate Reservoirs (ICCR), and for permission to publish this work  
 498 from the VSP project. We thank Andrew Curtis, Ian Main, Rachel Wood, and Giorgos  
 499 Papageorgiou at the University of Edinburgh, Tongcheng Han at the China University  
 500 of Petroleum, Qingdao, and Angus Best at the UK National Oceanography Center, Southamp-  
 501 ton, for their support in this work. The data on which this paper is based can be obtained  
 502 in Focke and Munn (1987), Verwer et al. (2008), Bakhorji (2010), and Fournier et al. (2011).

## 503 References

- 504 Akaike, H. (1973). Information theory and an extension of the maximum likelihood  
 505 principle. In B. N. Petrov & F. Csaki (Eds.), *Proceedings of the 2nd interna-*  
 506 *tional symposium on information theory* (Vol. 4, pp. 267–281).
- 507 Anselmetti, F. S., & Eberli, G. P. (1993). Controls on sonic velocity in carbonates.  
 508 *Pure and Applied geophysics*, *141*(2-4), 287–323.
- 509 Anselmetti, F. S., & Eberli, G. P. (1999). The velocity-deviation log: A tool to  
 510 predict pore type and permeability trends in carbonate drill holes from sonic  
 511 and porosity or density logs. *AAPG bulletin*, *83*(3), 450–466.
- 512 Aquino-López, A., Mousatov, A., & Markov, M. (2011). Model of sand formations  
 513 for joint simulation of elastic moduli and electrical conductivity. *Journal of*  
 514 *Geophysics and Engineering*, *8*(4), 568.
- 515 Aquino-López, A., Mousatov, A., Markov, M., & Kazatchenko, E. (2015). Modeling  
 516 and inversion of elastic wave velocities and electrical conductivity in elastic for-  
 517 mations with structural and dispersed shales. *Journal of Applied Geophysics*,  
 518 *116*, 28–42.

- 519 Archie, G. E. (1942). The electrical resistivity log as an aid in determining some  
520 reservoir characteristics. *Transactions of the AIME*, 146(1), 54–62.
- 521 Bakhorji, A. M. (2010). *Laboratory measurements of static and dynamic elastic*  
522 *properties in carbonate* (Unpublished doctoral dissertation). University of Al-  
523 berta.
- 524 Berryman, J. G. (1980). Long-wavelength propagation in composite elastic media II.  
525 Ellipsoidal inclusions. *The Journal of the Acoustical Society of America*, 68(6),  
526 1820–1831.
- 527 Berryman, J. G. (1992). Single-scattering approximations for coefficients in Biot’s  
528 equations of poroelasticity. *The Journal of the Acoustical Society of America*,  
529 91(2), 551–571.
- 530 Borai, A., et al. (1987). A new correlation for the cementation factor in low-porosity  
531 carbonates. *SPE Formation Evaluation*, 2(04), 495–499.
- 532 Burnham, K. P., & Anderson, D. R. (2002). *Multimodel inference: A practical*  
533 *information-theoretical approach* (2nd ed.). Colorado Cooperative Fish and  
534 Wildlife Research Unit, Colorado State University, Fort Collins, CO 80523-  
535 1484, USA: Springer-Verlag New York.
- 536 Burnham, K. P., & Anderson, D. R. (2004). Multimodel inference: Understand-  
537 ing aic and bic in model selection. *Sociological methods & research*, 33(2), 261–  
538 304.
- 539 Castagna, J. P., Batzle, M. L., & Kan, T. K. (1993). Rock physics - The link be-  
540 tween rock properties and avo response. In J. P. Castagna & M. M. Backus  
541 (Eds.), *Offset-dependent reflectivity - Theory and practice of AVO analysis:*  
542 *Investigations in Geophysics*. Society of Exploration Geophysicists.
- 543 Choquette, P. W., & Pray, L. C. (1970). Geologic nomenclature and classification of  
544 porosity in sedimentary carbonates. *American Association of Petroleum Geolo-*  
545 *gists Bulletin*, 54(2), 207–250.
- 546 Dunham, R. J. (1962). Classification of carbonate rocks according to depositional  
547 texture. In *Classification of carbonate rocks - a symposium* (pp. 108–121).  
548 U.S.: American Association of Petroleum Geologist.
- 549 Dvorkin, J., & Nur, A. (1996). Elasticity of high-porosity sandstones: Theory for  
550 two North Sea data sets. *Geophysics*, 61(5), 1363–1370.
- 551 Eberli, G. P., Baechle, G. T., Anselmetti, F. S., & Incze, M. L. (2003). Factors con-



- 552 trolling elastic properties in carbonate sediments and rocks. *The Leading Edge*,  
 553 *22*(7), 654–660.
- 554 Ellis, M., & Kirstetter, O. (2018). Resistivity anisotropic inclusion model for clastic  
 555 sediments. In *SEG technical program expanded abstracts 2018* (pp. 3488–3492).  
 556 Society of Exploration Geophysicists.
- 557 Eshelby, J. D. (1957). The determination of the elastic field of an ellipsoidal inclu-  
 558 sion, and related problems. *Proc. R. Soc. Lond. A*, *241*(1226), 376–396.
- 559 Focke, J. W., & Munn, D. (1987). Cementation exponents in Middle Eastern car-  
 560 bonate reservoirs. *SPE Formation Evaluation*, *2*(2), 155–167.
- 561 Fournier, F., Léonide, P., Biscarrat, K., Gallois, A., Borgomano, J., & Foubert, A.  
 562 (2011). Elastic properties of microporous cemented grainstones. *Geophysics*,  
 563 *76*(6), E211–E226.
- 564 Fournier, F., Léonide, P., Kleipool, L., Toullec, R., Reijmer, J. J. G., Borgomano,  
 565 J., ... Van Der Molen, J. (2014). Pore space evolution and elastic properties  
 566 of platform carbonates (Urgonian limestone, Barremian-Aptian, SE France).  
 567 *Sedimentary Geology*, *308*, 1–17.
- 568 Fournier, F., Pellerin, M., Villeneuve, Q., Teillet, T., Hong, F., Poli, E., ...  
 569 Hairabian, A. (2018). The equivalent pore aspect ratio as a tool for pore  
 570 type prediction in carbonate reservoirs. *AAPG Bulletin*, *102*(7), 1343.
- 571 Gassmann, F. (1951). *Verteljahrsschrift der naturforschenden gesellschaft in Zurich*.  
 572 *Über die elastizität poroser medien*, *96*, 1–23.
- 573 Gelius, L.-J., & Wang, Z. (2008). Modelling production caused changes in conductiv-  
 574 ity for a siliciclastic reservoir: A differential effective medium approach. *Geo-*  
 575 *physical Prospecting*, *56*(5), 677–691.
- 576 Glover, P. W. J. (2010). A generalized Archie’s law for n phases. *Geophysics*, *75*(6),  
 577 E247–E265.
- 578 Glover, P. W. J. (2016). Archie’s law - A reappraisal. *Solid Earth*, *7*(4), 1157.
- 579 Glover, P. W. J., Hole, M. J., & Pous, J. (2000). A modified Archie’s law for two  
 580 conducting phases. *Earth and Planetary Science Letters*, *180*(3-4), 369–383.
- 581 Han, D.-H., Nur, A., & Morgan, D. (1986). Effects of porosity and clay content on  
 582 wave velocities in sandstones. *Geophysics*, *51*(11), 2093–2107.
- 583 Han, T., Best, A. I., MacGregor, L. M., Sothcott, J., & Minshull, T. A. (2011). Joint  
 584 elastic-electrical effective medium models of reservoir sandstones. *Geophysical*

- 585         *Prospecting*, 59(4), 777–786.
- 586     Han, T., Clennell, M. B., Josh, M., & Pervukhina, M.     (2015).     Determination of  
587         effective grain geometry for electrical modeling of sedimentary rocks.         *Geo-*  
588         *physics*, 80(4), D319–D327.
- 589     Hill, R. (1952). The elastic behaviour of a crystalline aggregate. *Proceedings of the*  
590         *Physical Society. Section A*, 65(5), 349.
- 591     Humbert, P., & Plicque, F.     (1972).     Propriétés élastiques des carbonates rhom-  
592         bohédriques monocristallins: Calcite, magnésite et dolomie.     *Comptes Rendus*  
593         *de l'Académie des Sciences de Paris*, 275, 391–394.
- 594     Hurvich, C. M., & Tsai, C.-L. (1989). Regression and time series model selection in  
595         small samples. *Biometrika*, 76(2), 297–307.
- 596     Jeffreys, H. (1998). *The theory of probability*. OUP Oxford.
- 597     Kazatchenko, E., Markov, M., & Mousatov, A.     (2004).     Joint inversion of acous-  
598         tic and resistivity data for carbonate microstructure evaluation.     *Petrophysics*,  
599         45(02).
- 600     Kazatchenko, E., Markov, M., Mousatov, A., Pervago, E., et al. (2006). Simulation  
601         of the electrical resistivity of dual-porosity carbonate formations saturated  
602         with fluid mixtures. *Petrophysics*, 47(01).
- 603     Kittridge, M. G. (2014). Investigating the influence of mineralogy and pore shape on  
604         the velocity of carbonate rocks: Insights from extant global data sets. *Interpre-*  
605         *tation*, 3(1), SA15–SA31.
- 606     Kullback, S., & Leibler, R. A. (1951). On information and sufficiency. *The annals of*  
607         *mathematical statistics*, 22(1), 79–86.
- 608     Kuster, G. T., & Toksöz, M. N. (1974). Velocity and attenuation of seismic waves  
609         in two-phase media: Part I. Theoretical formulations. *Geophysics*, 39(5), 587–  
610         606.
- 611     Man, C.-S., & Huang, M. (2011). A simple explicit formula for the Voigt-Reuss-Hill  
612         average of elastic polycrystals with arbitrary crystal and texture symmetries.  
613         *Journal of Elasticity*, 105(1-2), 29–48.
- 614     Markov, M., Kazatchenko, E., Mousatov, A., et al. (2004). Prediction of the acous-  
615         tic velocities, electrical and thermal conductivities of carbonate formations  
616         applying self-consistent methods. In *SPWLA 45th annual logging symposium*.
- 617     Mavko, G., Mukerji, T., & Dvorkin, J. (2009). *The rock physics handbook: Tools for*

- 618           *seismic analysis of porous media*. Cambridge University Press.
- 619 Mendelson, K. S., & Cohen, M. H. (1982). The effect of grain anisotropy on the elec-  
620           trical properties of sedimentary rocks. *Geophysics*, *47*(2), 257–263.
- 621 Mukerji, T., Berryman, J., Mavko, G., & Berge, P. (1995). Differential effective  
622           medium modeling of rock elastic moduli with critical porosity constraints. *Geo-  
623           physical Research Letters*, *22*(5), 555–558.
- 624 Neustaedter, R. H. (1968). Log evaluation of deep ellenburger gas zones. In *Spe deep  
625           drilling and development symposium*.
- 626 Nigmatullin, R., Dissado, L., & Soutougin, N. (1992). A fractal pore model for  
627           Archie’s law in sedimentary rocks. *Journal of Physics D: Applied Physics*,  
628           *25*(1), 32.
- 629 Norris, A. N. (1985). A differential scheme for the effective moduli of composites.  
630           *Mechanics of materials*, *4*(1), 1–16.
- 631 Nur, A., Mavko, G., Dvorkin, J., & Galmudi, D. (1998). Critical porosity: A key  
632           to relating physical properties to porosity in rocks. *The Leading Edge*, *17*(3),  
633           357–362.
- 634 Nur, A. M., Mavko, G., Dvorkin, J., & Gal, D. (1995). Critical porosity: The key to  
635           relating physical properties to porosity in rocks. In *SEG technical program ex-  
636           panded abstracts 1995* (pp. 878–881). Society of Exploration Geophysicists.
- 637 Pickett, G. R. (1963). Acoustic character logs and their applications in formation  
638           evaluation. *Journal of Petroleum technology*, *15*(06), 659–667.
- 639 Pride, S. R., Berryman, J. G., Commer, M., Nakagawa, S., Newman, G. A., &  
640           Vasco, D. W. (2017). Changes in geophysical properties caused by fluid in-  
641           jection into porous rocks: analytical models. *Geophysical Prospecting*, *65*(3),  
642           766–790.
- 643 Raftery, A. E. (1996). Approximate Bayes factors and accounting for model uncer-  
644           tainty in generalised linear models. *Biometrika*, *83*(2), 251–266.
- 645 Raymer, L. L., Hunt, E. R., & Gardner, J. S. (1980). An improved sonic transit  
646           time-to-porosity transform. In *SPWLA 21st annual logging symposium*.
- 647 Saleh, A. A., & Castagna, J. P. (2004). Revisiting the Wyllie time average equation  
648           in the case of near-spherical pores. *Geophysics*, *69*(1), 45–55.
- 649 Salem, H. S., & Chilingarian, G. V. (1999). The cementation factor of Archie’s  
650           equation for shaly sandstone reservoirs. *Journal of Petroleum Science and En-*

- 651            *gineering*, 23(2), 83–93.
- 652    Sen, P. N., Scala, C., & Cohen, M. H.    (1981).    A self-similar model for sedimen-  
653            tary rocks with application to the dielectric constant of fused glass beads. *Geo-*  
654            *physics*, 46(5), 781–795.
- 655    Simmons, G. (1965). *Single crystal elastic constants and calculated aggregate proper-*  
656            *ties* (Tech. Rep.). Dallas, Texas: Southern Methodist University.
- 657    Szu, H., & Hartley, R. (1987). Fast simulated annealing. *Physics letters A*, 122(3-4),  
658            157–162.
- 659    Tosaya, C. (1982). *Acoustical properties of clay-bearing rocks* (Unpublished doctoral  
660            dissertation). Stanford University.
- 661    Vernik, L., & Nur, A.    (1992).    Ultrasonic velocity and anisotropy of hydrocarbon  
662            source rocks. *Geophysics*, 57(5), 727–735.
- 663    Verwer, K., Braaksma, H., & Kenter, J. A.    (2008).    Acoustic properties of car-  
664            bonates: Effects of rock texture and implications for fluid substitution.    *Geo-*  
665            *physics*, 73(2), B51–B65.
- 666    Verwer, K., Eberli, G. P., & Weger, R. (2011). Effect of pore structure on electrical  
667            resistivity in carbonates. *AAPG bulletin*, 95(2), 175–190.
- 668    Waxman, M. H., & Smits, L. J. M. (1968). Electrical conductivities in oil-bearing  
669            shaly sands. *Society of Petroleum Engineers Journal*, 8(02), 107–122.
- 670    Winsauer, W. O., Shearin Jr, H., Masson, P., & Williams, M. (1952). Resistivity  
671            of brine-saturated sands in relation to pore geometry.    *AAPG bulletin*, 36(2),  
672            253–277.
- 673    Wu, T. T. (1966). The effect of inclusion shape on the elastic moduli of a two-phase  
674            material. *International Journal of Solids and Structures*, 2(1), 1–8.
- 675    Xu, S., & Payne, M. A. (2009). Modeling elastic properties in carbonate rocks. *The*  
676            *Leading Edge*, 28(1), 66–74.
- 677    Zimmerman, R. W. (1991). *Compressibility of sandstones* (Vol. 29). Elsevier.